


# Multi-chronometer dating of the Souter Head complex: rapid exhumation terminates the Grampian Event of the Caledonian Orogeny

Darren F. MARK<sup>1,2\*</sup> , Clive M. RICE<sup>3</sup>, Malcolm HOLE<sup>3</sup> and Dan CONDON<sup>4</sup>

<sup>1</sup> Isotope Geoscience Unit, Scottish Universities Environmental Research Centre, Rankine Avenue, East Kilbride, Scotland, G75 0QF, UK

<sup>2</sup> Department of Earth & Environmental Science, University of St Andrews, St Andrews, KY16 9AJ, UK

<sup>3</sup> Department of Geology & Petroleum Geology, University of Aberdeen, Aberdeen, AB24 3UE, UK

<sup>4</sup> NERC Isotope Geosciences Laboratory, British Geological Survey, Keyworth, NG12 5GG, UK

\* Corresponding author. Email: [Darren.Mark@glasgow.ac.uk](mailto:Darren.Mark@glasgow.ac.uk)

**ABSTRACT:** The Souter Head sub-volcanic complex (Aberdeenshire, Scotland) intruded the high-grade metamorphic core of the Grampian Orogen at  $469.1 \pm 0.6$  Ma (uranium-238–lead-206 ( $^{238}\text{U}$ – $^{206}\text{Pb}$ ) zircon). It follows closely peak metamorphism and deformation in the Grampian Terrane and tightly constrains the end of the Grampian Event of the Caledonian Orogeny. Temporally coincident U–Pb and argon/argon ( $^{40}\text{Ar}/^{39}\text{Ar}$ ) data show the complex cooled quickly with temperatures decreasing from *ca.*800 °C to less than 200 °C within 1 Ma. Younger rhenium–osmium (Re–Os) ages are due to post-emplacment alteration of molybdenite to powellite. The U–Pb and Ar/Ar data combined with existing geochronological data show that D2/D3 deformation, peak metamorphism (Barrovian and Buchan style) and basic magmatism in NE Scotland were synchronous at *ca.*470 Ma and are associated with rapid uplift ( $5$ – $10$  km  $\text{Ma}^{-1}$ ) of the orogen, which, by *ca.*469 Ma, had removed the cover to the metamorphic pile. Rapid uplift resulted in decompressional melting and the generation of mafic and felsic magmatism. Shallow slab break-off (50–100 km) is invoked to explain the synchronicity of these events. This interpretation implies that peak metamorphism and D2/D3 ductile deformation were associated with extension. Similarities in the nature and timing of orogenic events in Connemara, western Ireland, with NE Scotland suggest that shallow slab break-off occurred in both localities.



**KEY WORDS:**  $^{40}\text{Ar}/^{39}\text{Ar}$ , granite, Ireland, Re–Os, Scotland, U–Pb.

The Caledonides of Britain and Ireland have inspired numerous studies, many of fundamental importance, seeking to understand orogenic processes. Central to this aim is providing a robust geochronological framework to test prospective tectonothermal models. There is a large geochronological database for the Grampian Event of the Caledonian Orogeny (referred to as the Grampian Event from now) based on the ages of metamorphic minerals (*in situ* and detrital) and syn- and post-orogenic intrusions (Friedrich *et al.* 1999; Oliver 2001; Baxter *et al.* 2002; Dewey 2005; Oliver *et al.* 2008; Viète *et al.* 2013). Despite this considerable geochronological framework, which is accompanied by detailed field, geochemical and isotopic studies that have spawned a plethora of plate tectonic models, the causes of the rapid, synchronous, Grampian orogenic peak remain enigmatic (Ague & Baxter 2007; Chew & Strachan 2013). Here, we present a multi-chronometer study of an Ordovician sub-volcanic intrusion at Souter Head near Aberdeen, which is emplaced within the high-grade Barrovian core of the Grampian Orogen. The Souter Head sub-volcanic complex (SHSC) was emplaced immediately following main-stage deformation and provides a unique opportunity to test cause-and-effect processes/relationships at the termination of the Grampian Event.

The multi-chronometer (argon/argon ( $^{40}\text{Ar}/^{39}\text{Ar}$ ), uranium-238–lead-206 ( $^{238}\text{U}$ – $^{206}\text{Pb}$ ), rhenium–osmium (Re–Os)) approach facilitates the construction of a detailed temporal framework for

the SHSC. The data yield insights into structural changes associated with the termination of the Grampian Event and through comparison with numerical simulations and modern-day subduction zones, highlight that shallow slab break-off (50–100 km) explains the synchronicity of events occurring across the subduction zone in Ireland and Scotland.

## 1. Geological background

Neoproterozoic–Cambrian Dalradian sediments were deposited on the passive margin of the Laurentian continent and deformed and metamorphosed during the Grampian Event following a continent-arc collision (Chew & Strachan 2013 and references therein). In the following, we summarise the sequences of events in terms of the onset of orogenesis, the timing of deformation and the termination of the event.

### 1.1. Onset of the Grampian Event

The rocks of the Grampian Terrane are continuous between NE Scotland and Connemara, western Ireland (Fig. 1), and are likely the telescoped end-result of contraction of a passive margin. A maximum age for the start of the Grampian Event was suggested using the age (*ca.*478 Ma) of the youngest deformed Dalradian sedimentary rocks (assuming the Dalradian extends into the Ordovician; Tanner 2014 and references therein).

A minimum pre-early Silurian age is demonstrated in Connemara, where Upper Llandovery strata rest unconformably on Dalradian sediments (McKerrow & Campbell 1960; Soper *et al.* 1999). The *ca.*478 Ma age of Tanner (2014) may well be correct but this constraint does not preclude deformation having been initiated further outboard in the subduction zone significantly earlier.

Ophiolites (dismembered and ophiolites *sensu stricto*), located at Unst, Bute, Tyrone and Clew Bay (Spray & Dunning 1991; Chew *et al.* 2010; Crowley & Strachan 2015) (Fig. 1a, b) are slices of oceanic-type lithosphere that formed in supra-subduction zone arc-forearc environments prior to orogenesis, and were subsequently obducted onto a colliding passive margin. As such, they record the initial stages in the closure of the Iapetus Ocean (e.g., Chew *et al.* 2010), and the determination of accurate (cooling)-ages for these ophiolites would provide additional constraints on the timing of onset of deformation. In comparison to Tanner (2014), these ages should pre-date *ca.*478 Ma. Ages obtained from the metamorphic soles of these ophiolites suggest that obduction was initiated at  $490 \pm 4$  (Clew Bay; Chew *et al.* 2010),  $492 \pm 1$  Ma (Bute; Chew *et al.* 2010),  $484 \pm 4$  Ma (Unst; Crowley & Strachan 2015) and  $492 \pm 3$  Ma (Unst; Spray & Dunning 1991). There is also an age constraint ( $477.6 \pm 1.9$  Ma, samarium–neodymium (Sm–Nd) garnet) for the ophiolite at Ballantrae (Stewart *et al.* 2017). However, this site (Fig. 1b), which is located on the opposite side of the Midland Valley Arc to the other ophiolite complexes, potentially relates to a different and younger phase of the collision event and, thus, the data are not considered further. Recently, Johnson *et al.* (2017) proposed the existence of an island arc that may be temporally associated with ophiolite obduction. However, the large age uncertainties reported by Johnson *et al.* (2017) ( $\pm 8$ – $9$  Ma) and scatter in the data mean the relationship, if any, of this island arc to the onset of the Grampian Event is unclear.

Although, locally, the onset of the Grampian Event (and any orogenic collision) was likely to have been diachronous, large age uncertainties (e.g., in excess of 2 Ma) mean that we currently lack the temporal resolution to dissect the evolution of the orogenesis. Therefore, the best age for the onset of the Grampian Event is calculated by taking the weighted average of the ophiolite age constraints (Clew Bay, Bute, Unst) and accounting for the scatter in the data by reporting the age with an uncertainty that is multiplied by the square-root of the mean square weighted deviates (MSWD, or reduced chi-squared). This approach suggests that Grampian Event deformation commenced at  $491 \pm 2$  Ma.

## 1.2. Grampian deformation and magmatism

Four phases of deformation are commonly recognised in NE Scotland (D1 to D4), of which the first three include the main compressional and nappe-building phases (Chew & Strachan 2013). Multiple phases of deformation are found in the various Dalradian inliers in Ireland but these cannot be correlated accurately with NE Scotland. Barrovian-style metamorphism is found throughout this sector. Buchan-style metamorphism is restricted to the Buchan block in NE Scotland and southern Connemara, in conjunction with syn- and post-orogenic intrusions (granites and voluminous basic intrusions) (Chew & Strachan 2013). Amongst these intrusions are foliated gabbros and granites (e.g., Insch and Strichen), which attest to emplacement pre- or syn-deformation. The intrusions yield similar U–Pb and Ar/Ar radioisotopic ages for peak regional metamorphism and deformation at *ca.*475–470 Ma (Kneller & Aftalion 1987; Friedrich *et al.* 1999; Dempster *et al.* 2002; Oliver *et al.* 2008). High-grade pelites also yield Ar/Ar and U–Pb ages for peak metamorphism in this range (Viète *et al.* 2013; Vorhies *et al.* 2013).

In the Glen Clova area of Scotland (Fig. 1c), younger radioisotopic (e.g., Sm–Nd garnet) ages suggest continued metamorphism

and deformation to  $464.8 \pm 2.7$  Ma (2-sigma, analytical precision) (Baxter *et al.* 2002; Viète *et al.* 2013; Vorhies *et al.* 2013). However, this datum (Baxter *et al.* 2002) is the rim age of one garnet derived from the weighted subtraction of an ‘inferred’ garnet core age from a measured bulk garnet age. This model date likely reflects mixing and requires an unlikely assumption of constant Nd concentration across the duration of garnet growth (*ca.*8 Ma) and, as such, we do not consider this age constraint further. Baxter *et al.* (2002) reported a bulk garnet age of  $466.8 \pm 1.9$  Ma (2-sigma, analytical precision). This age with associated decay-constant uncertainty incorporated to allow for inter-chronometer comparison is  $466.8 \pm 3.2$  Ma, and we contend this is the most accurate minimum age constraint for syn- to slightly post-D3 deformation at Glen Clova (based on the textural analyses of McLellan 1985, 1989).

## 1.3. Termination of the Grampian Orogeny

The ages of unfoliated intrusions (post-deformation) currently provide the best constraints for the termination of orogenesis, including the Oughterard granite in western Ireland ( $463 \pm 3$  Ma; Friedrich *et al.* 1999), the Kennethmont granite in NE Scotland ( $457 \pm 1$  Ma; Oliver *et al.* 2000) and an undeformed quartzo-feldspathic pegmatite ( $474 \pm 5$  Ma) at Portsoy, also in NE Scotland (Carty *et al.* 2012) (Fig. 1b). The non-foliated Cove granite ( $458 \pm 5$  Ma) and the Nigg Bay granite ( $465 \pm 5$  Ma) are also located in NE Scotland (Appleyby *et al.* 2010).

## 2. The SHSC

The SHSC is emplaced in metasedimentary rocks of the Dalradian Aberdeen Formation (Southern Highland Group) on the coast between Aberdeen and Findon (Fig. 1b, d), 10 km S of the foliated Aberdeen Granite ( $470 \pm 2$  Ma; Kneller & Aftalion 1987). The formation is well exposed along this stretch of coastline, whereas, inland, exposure is generally poor (Munro 1986). The SHSC is also on the southern edge of a granite vein complex occupying a large area S of the Dee fault (Fig. 1d). This fault separates the complex from the foliated Aberdeen Granite (Kneller & Aftalion 1987).

Much of the granite in the complex is migmatitic and typically occurs as lenses and sheets at the cm- to 10 m-scale. Larger bodies do occur and the weakly foliated (magmatic foliation) granite at Nigg Bay (Fig. 1d) has been dated at  $465 \pm 5$  Ma (Appleyby *et al.* 2010). The unfoliated Cove granite to the S of the complex is dated at  $458 \pm 5$  Ma (Fig. 1d) (Appleyby *et al.* 2010). Kneller & Aftalion (1987) distinguished granite veins in the complex ranging in structural age from pre D3 or syn D3 to post D3, and concluded that (1) the foliated Aberdeen granite is ‘broadly’ syn D3, and (2) that the veins and larger bodies of granite represent a period of intrusion that overlapped D3. Unfoliated granites in the complex are, therefore, post D3. The geochronological age of the SHSC at *ca.*469 Ma is discussed in this structural and magmatic context.

The SHSC lies in the sillimanite zone of Barrovian metamorphism (Fig. 1c) (Kneller & Gillen 1987). The metamorphic grade increases systematically from the Highland Boundary Fault (HBF) northwards. Peak metamorphism (sillimanite grade) is reached at Findon, 4 km S of the SHSC (Harte *et al.* 1987), and Munro (1986) records sillimanite as being widespread in the Aberdeen Formation. Sillimanite is reported also in the syn D3 Aberdeen granite (Mackie 1926). Thus, we conclude that the SHSC host rocks are within the sillimanite zone.

Exposure of the SHSC reveals a multistage history of repeated intrusion, breccia formation, hydrothermal activity, mineralisation and faulting (Rice & Mark 2019). Two-mica granites and intrusive breccia are the dominant rock types, with minor pegmatite, quartz porphyry, felsite and dolerite. There is an inner

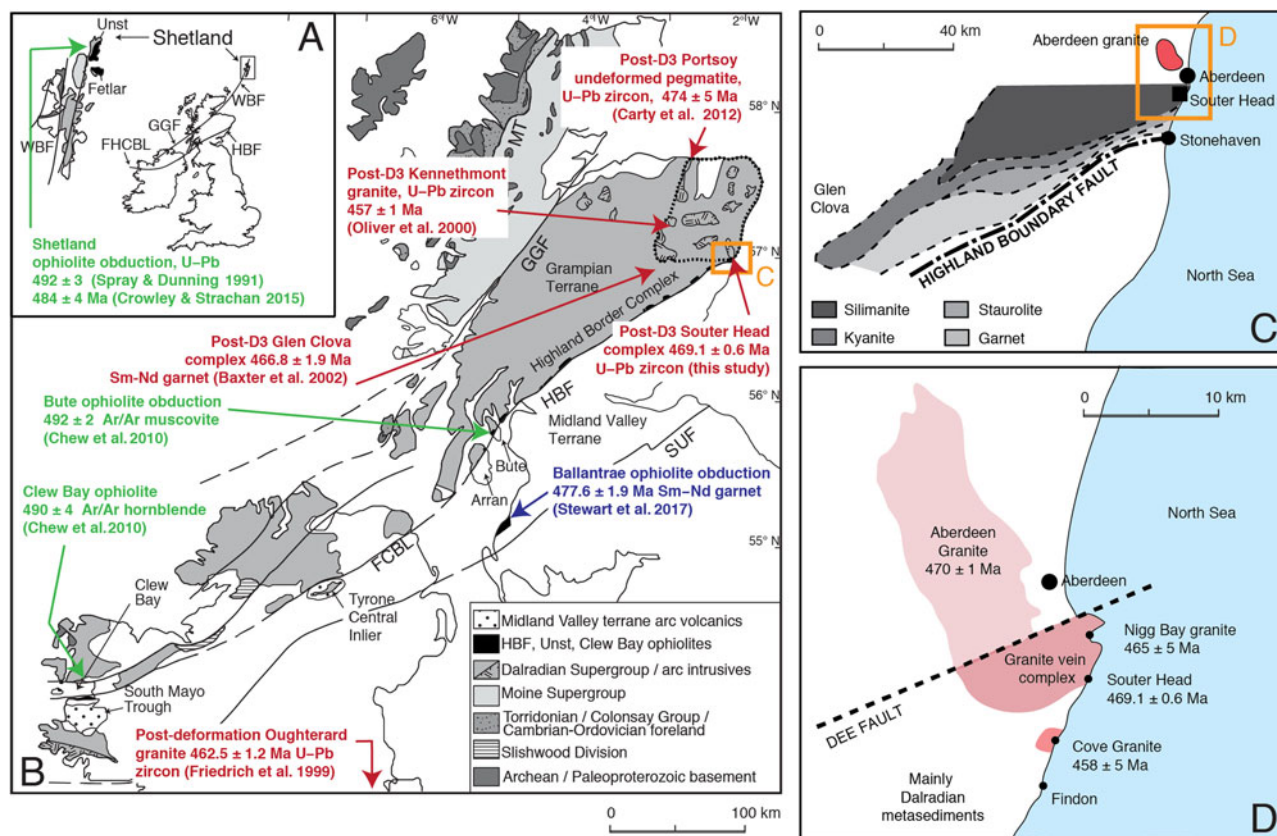


**Figure 1** (A) Map of the UK showing constraints from ophiolite obduction on Shetland for the onset of Grampian orogenesis:  $492 \pm 3$  and  $484 \pm 4$  Ma (Spray & Dunning 1991; Crowley & Strachan 2015, respectively). (B) Figure showing the timing of onset (green) and termination (red) of Grampian orogenesis in Scotland and Ireland: Unst ophiolite obduction,  $492 \pm 3$  Ma (Spray & Dunning 1991) and  $484 \pm 4$  Ma (Crowley & Strachan 2015); Clew Bay ophiolite obduction  $490 \pm 4$  Ma (Chew *et al.* 2010); Bute ophiolite obduction,  $492 \pm 2$  Ma (Chew *et al.* 2010). The blue box shows Ballantrae ophiolite obduction  $477.6 \pm 1.9$  Ma (Stewart *et al.* 2017); however, this event may not be related to the Grampian Event (see discussion). Figure modified from Chew *et al.* 2010. (C) Location of Souter Head in relation to the Barrovian metamorphic zones (modified from fig. 1 of Baxter *et al.* 2002) and the Aberdeen Granite. (D) The location and ages of granites located close to Aberdeen.

sequence (described by Porteous 1973) separated by faults from two previously undescribed outer granites (Burnbanks and Bunstane; Fig. 2). In addition, there is widespread quartz veining, associated hydrothermal alteration and localised molybdenite mineralisation. The SHSC has been interpreted as sub-volcanic and, in the absence of a significant foliation, temporally linked to the Silurian–Devonian Newer Granites (Porteous 1973; Kneller & Gillen 1987) that span the period of late Caledonian orogenic convergence and uplift (Strachan *et al.* 2002; Oliver *et al.* 2008).

The relative timing of crystallisation for the members of the inner sequence of the SHSC can be established from intrusive relationships to be, from oldest to youngest, (1) intrusive breccia, (2) two mica granites, (3) pegmatite, (4) quartz porphyry and (5) most quartz veins. Felsite dykes are coeval with the SHSC and dolerite is younger, but these intrusive rocks occur regionally and are not genetically linked to the SHSC.

Intrusive breccia occurs as three main masses separated by granite (Fig. 2). Rare original contacts show that granite intrudes the breccia. Breccia clasts are mainly angular semi-pelite with rare rounded granite. Maximum clast dimensions are typically 10–20 cm, but can range up to 30 m. The northern granite mass contains xenoliths of semi-pelite and rare amphibolite, and exhibits a weak and patchy foliation defined by the alignment of biotite grains. The foliation is interpreted as magmatic since the biotite is enclosed by non-aligned minerals with an igneous texture (Paterson *et al.* 1989). In contrast, the southern mass is non-xenolithic and lacks any foliation (as do all other units in the inner sequence), indicating emplacement post-D3 deformation. The xenolithic granite is interpreted as the

marginal facies of the non-xenolithic granite, which likely explains the foliation.

Pegmatites cut the two granites and breccias, and are composed of quartz, K-feldspar, muscovite and biotite. They occur mainly as linear veins that extend up to 70 m along strike. With the exception of the dolerite, quartz veins cut all of the intrusive rocks. The quartz veins are generally straight-sided, massive and can be traced for up to 130 m. They mostly strike N–S and are either vertical or dip easterly at a shallow angle. One of these veins that extends for over 50 m and cuts the breccia, non-xenolithic granite and quartz porphyry contains thin margin-parallel bands and clusters of intergrown muscovite and molybdenite (Fig. 3).

## 2.1. Structural age of the SHSC

The structural age of the SHSC cannot be obtained by examination of the contacts between the metasediments and the outer granites or the inner sequence due to lack of exposure or accessible exposure (Rice & Mark 2019). However, constraints can be placed upon it by (1) assuming that N–S-striking quartz veins cutting metasediments N of Souter Head are the same age as similarly orientated veins in the SHSC, (2) examining truncated structures in clasts and xenoliths in the SHSC and (3) comparing the structures in the SHSC with those in better exposed areas (Appendix DM1).

**2.1.1. Quartz veins.** N–S-striking quartz veins cut the metasediments in the Altens Haven area and are demonstrably post D1. Since they lack significant deformation, they were emplaced late in the structural sequence and are probably post D3. If these veins are related to the late N–S-striking veins in the SHSC, the latter are also likely post D3.

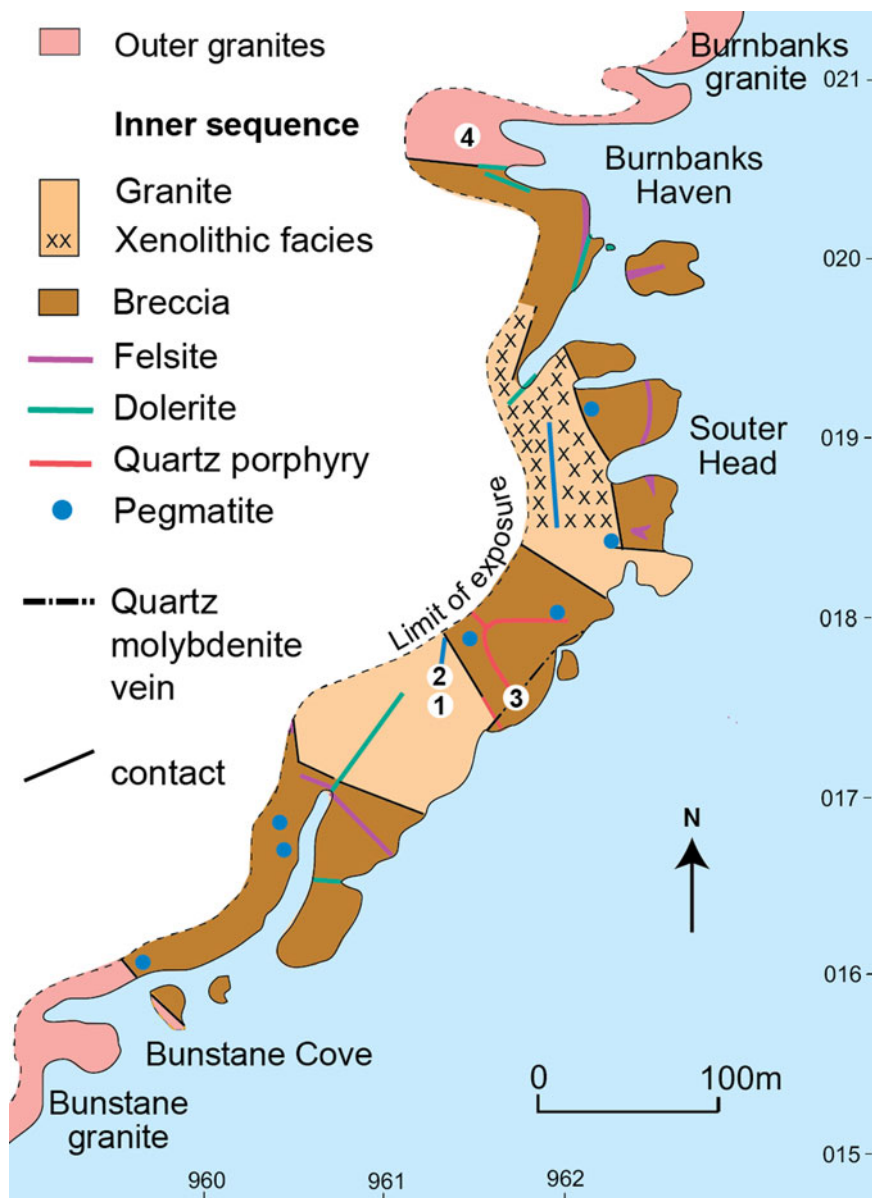


**Figure 2** Simplified geological map of the Souter Head complex and the sample localities (1–4). Also see Rice & Mark (2019) for further information. Sample location (1) zircon and muscovite from the inner non-xenolithic granite; sample location (2) K-feldspar and muscovite from pegmatite cutting the non-xenolithic granite; sample location (3) intergrown and coeval muscovite and molybdenite from the late quartz–molybdenite vein; sample location (4) muscovite from the outer Burnbanks granite.

**2.1.2. Clasts and xenoliths in the SHSC.** The structural age of the SHSC must be younger than any structures seen in clasts and xenoliths that are truncated at the margins. Most clasts and xenoliths are semi-pelites like the country rocks and possess a fabric identical in character to the country rocks (Appendix DM1). In keeping with the general lack of folding in the host rocks, the fabric is planar, even in the 30 m rafts. There is rare cm-scale folding of this fabric, placing the SHSC as post D2 or D3.

**2.1.3. Comparison with other areas.** The absence of a tectonic foliation suggests the SHSC is of a comparable structural age (post D3) to the late unfoliated granite veins elsewhere in the granite vein complex, which cut D3 structures (Kneller & Aftalion 1987). The other evidence presented above is consistent with this conclusion.

### 3. Samples

$^{40}\text{Ar}/^{39}\text{Ar}$ ,  $^{238}\text{U}$ – $^{206}\text{Pb}$  and Re–Os dating were used to construct a chronological framework for the inner sequence and an outer

granite of the SHSC (Fig. 2), together with a late molybdenite-bearing quartz vein (Fig. 3). The chronology for the inner sequence, which lacks a tectonic foliation, provides a chronological marker for the termination of peak metamorphism and deformation in the Grampian Event in NE Scotland (Rice & Mark 2019). Further, the chronology, integrated with the structural setting and metamorphic grade, permits interrogation of subduction zone response (i.e., topographical change, exhumation) during the termination of the Grampian Event. Such investigations are possible due to the excellent field relations exposed in the Souter Head coastal transect, which provide a robust petrogenetic framework and a wide variety of dating targets. Specifically, we targeted muscovite from the outer Burnbanks granite (sample location 4, Fig. 2), zircon and muscovite from the inner non-xenolithic granite (sample location 1, Fig. 2), K-feldspar and muscovite from pegmatite cutting the non-xenolithic granite (sample location 2, Fig. 2) and, finally, intergrown and demonstrably coeval muscovite and molybdenite from the late quartz–molybdenite vein (sample location 3, Figs 2, 3).



**Figure 3** Field photograph showing the targeted quartz–molybdenite vein hosted by intrusive breccia (sample point 3 in Fig. 2). Non-xenolithic granite can be observed in the background. Black arrows show molybdenite- and muscovite-rich grey streaks through the vein.

### 3.1. Petrography of the late muscovite–molybdenite-bearing quartz vein

The dominant mineral is quartz, of which three types can be distinguished in cathodoluminescence (CL) (Fig. 4). The most common and earliest is medium grey in CL. This has recrystallised to grains in the size range 0.1–5.0 mm. In places, primary oscillatory zoning is preserved (Fig. 4a). A network of dark quartz, which follows the grain boundaries and fills fractures, postdates this quartz (Fig. 4a, b). The third and latest is margin-parallel bright-quartz veinlets. These, and fracture-controlled inclusion trails, both crosscut the network (Fig. 4).

Molybdenite shows a close spatial and temporal relationship with muscovite. The two minerals are mainly found in clusters with muscovite and molybdenite crystals up to 2 mm and 0.4 mm, respectively. In the clusters, molybdenite occurs between muscovite crystals, but also crosscutting crystals and along muscovite cleavages (Fig. 4d). The siting of the clusters is closely linked to the dark quartz network (Fig. 4a). Lesser amounts of molybdenite and muscovite are found in margin-parallel veinlets (Fig. 4b, c) and dispersed in the dark-quartz network. In these last two locations, the molybdenite and muscovite are finer grained (typically up to 150  $\mu\text{m}$ ). The close spatial association of molybdenite with muscovite within the dark quartz network suggests all three minerals are broadly coeval.

## 4. Methods

### 4.1. $^{40}\text{Ar}/^{39}\text{Ar}$ dating

Samples for  $^{40}\text{Ar}/^{39}\text{Ar}$  dating were prepared using the methodologies outlined in Mark *et al.* (2011). Briefly, samples were crushed and subjected to magnetic separation. The sericite-

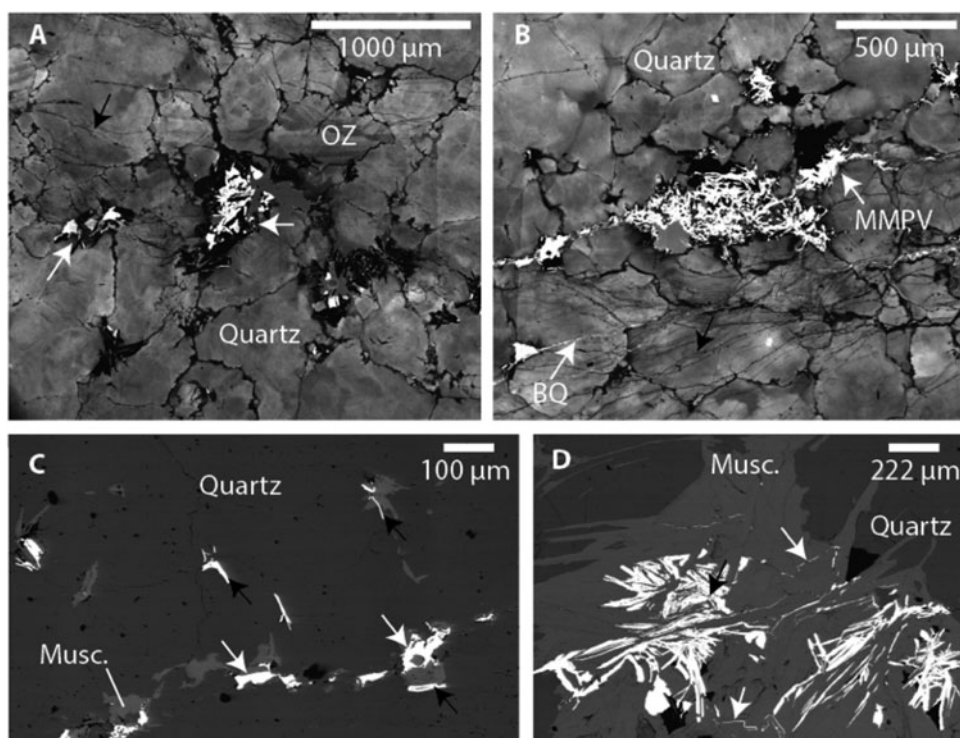


**Figure 4** (A) SEM-CL: typical fracture network of dark quartz in quartz vein partly following the boundaries of recrystallised quartz crystals (medium grey). Clusters of molybdenite and muscovite (white arrows) are located in the network of dark quartz, the white mineral in the clusters is powellite. Note, in SEM-CL the molybdenite and muscovite are not visible, but are shown in Back Scattered Electron Microscope (BSEM) (Figs 3d, 4c, d). Finer lines corresponding to fluid inclusion trails are arrowed (black) and an area of primary oscillatory zoning in quartz is marked (OZ). (B) SEM-CL: medium-grey quartz with network of dark quartz and margin-parallel (running E–W) veinlet (MPV) containing muscovite and molybdenite (opaque) and powellite (white). Fine lines corresponding to fluid inclusion trails (black arrow) and quartz veinlet (BQ) cut the network. (C) SEM-CL: margin-parallel veinlet in quartz (dark grey) composed of muscovite (medium grey), molybdenite (black arrows) and powellite (white arrows). Small clusters of molybdenite and muscovite and isolated crystals of these two minerals are also present. (D) BSEM: molybdenite–muscovite cluster. Molybdenite (black arrows) is located between muscovite (medium grey) crystals and cleavages and also cross-cutting muscovite crystals and cleavages. Fine veinlets of powellite (white arrows) are present, cutting muscovite.

bearing fraction was run down a shaking table and relatively pure muscovite splits collected. K-feldspar samples were purified using heavy liquids and cleaned by leaching in 5% Hydrofluoric acid (HF) for 2 min. Subsequently, clean grains (no visible inclusions) were hand-picked under a binocular microscope with all samples (wafers and separates) further cleaned in ethanol and deionised water.

Samples were parcelled in high-purity aluminium discs for irradiation. Standards Fish Canyon sanidine (FCs-EK; Morgan *et al.* 2014) ( $28.294 \pm 0.036$  Ma; Renne *et al.* 2011), GA1550 biotite ( $99.738 \pm 0.104$  Ma; Renne *et al.* 2011) and Hb3gr ( $1081.0 \pm 1.2$  Ma; Renne *et al.* 2011) hornblende were loaded adjacent to the samples to permit accurate characterisation of the neutron flux (J-parameter). Samples were irradiated for 2700 min in the Cadmium-lined facility of the CLICIT Facility at the Oregon State University TRIGA reactor. Standards were analysed on a MAP 215-50 system (described below briefly and in more detail by Mark *et al.* 2011) – FCs was analysed by carbon dioxide (CO<sub>2</sub>) laser total fusion as single crystals ( $n = 20$ ), GA1550 ( $n = 5$ ) and Hb3gr ( $n = 5$ ) were step-heated using a CO<sub>2</sub> scanning laser (e.g., Barfod *et al.* 2014). Using GA1550, the J-parameter was determined to a precision *ca.* 0.1% uncertainty. Using the J-parameter measurements from GA1550, ages were determined for FCs and Hb3gr. The ages overlapped at the 68% confidence (1-sigma) with the ages reported by Renne *et al.* (2011), showing the J-parameters determined from GA1550 to be accurate.

The samples were step-heated using a CO<sub>2</sub> laser (approximately 500–1500 °C, optical pyrometer measurements). Extracted gases were subjected to 300 s of purification by exposure to two SAES GP50 getters (one maintained at room temperature, the other held at *ca.* 450 °C). A cold finger was maintained at –95.5 °C using a mixture of dry ice (CO<sub>2</sub>[s]) and acetone. Ion beam intensities (i.e., Ar isotope intensities and, hence, ratios) were measured using a GVI ARGUS V noble gas mass spectrometer in ‘true’ multicollection mode (Mark *et al.* 2009). Faraday cups ( $10^{11}$  ohm <sup>40</sup>Ar,  $10^{12}$  ohm <sup>39–36</sup>Ar) were used to make measurements. The system had a measured sensitivity of  $7.40 \times 10^{-14}$  moles Volt<sup>-1</sup>. The extraction and clean-up, as well as mass spectrometer inlet and measurement protocols and data acquisition, were automated. Backgrounds (full extraction line and mass spectrometer) were made following every two analyses of unknowns. The average background  $\pm$  standard deviation ( $n = 162$ ) from the entire run sequence was used to correct raw isotope measurements from unknowns and air pipettes. Mass discrimination was monitored by analysis of air pipette aliquots after every five analyses of unknowns ( $n = 63$ ,  $7.32 \times 10^{-14}$  moles <sup>40</sup>Ar, <sup>40</sup>Ar/<sup>36</sup>Ar =  $299.81 \pm 0.19$ ).

All Ar isotope data were corrected for backgrounds, mass discrimination and reactor-produced nuclides, and processed using standard data reduction protocols (e.g., Mark *et al.* 2005) and reported according to the criteria of Renne *et al.* (2009). The atmospheric argon isotope ratios of Lee *et al.* (2006), which have been independently verified by Mark *et al.* (2011), were employed. The ages were calculated using the optimisation model approach of Renne *et al.* (2010) using the parameters of Renne *et al.* (2011). The <sup>40</sup>Ar/<sup>39</sup>Ar ages are reported as  $X \pm Y/Z$ , where  $Y$  is the analytical uncertainty and  $Z$  is the full external precision, including uncertainties from the decay constant. All ages are reported at the 2-sigma confidence interval.

## 4.2. Isotope dilution thermal ionisation mass spectrometry (ID-TIMS) U–Pb geochronology

Zircons were hand-picked after separation using conventional techniques. Analyses were performed at the NERC Isotope Geosciences Laboratory (NIGL) at the British Geological Survey, Keyworth, UK, following established protocols (e.g.,

Noble *et al.* 2014). This includes a chemical abrasion procedure (Mattinson 2005) and U/Pb determinations calibrated using the EARTHTIME (ET535) tracer solution (Condon *et al.* 2015; CA-ID-TIMS). For data reduction and uncertainty propagation, we followed the strategy of Bowring & McLean (2011) and McLean *et al.* (2011).

As we are not dealing with geologically ‘young’ rocks and, thus, our data will not be precise enough to concern ourselves with ‘over-interpretation’ of the zircon U–Pb age data (i.e., youngest zircon versus weighted mean age; Ickert *et al.* 2015; Mark *et al.* 2017), we used a weighted mean of the youngest population of each sample. Each youngest population contained three or more ages that give an MSWD that is acceptable for a single population (Wendt & Carl 1991). The <sup>206</sup>Pb/<sup>238</sup>U ages presented in this paper are corrected for initial Thorium (Th) disequilibrium and uncertainties are quoted at the 2-sigma confidence level, unless stated otherwise. Uncertainties are listed as  $\pm X/Y/Z$ , where  $X$  is the analytical uncertainty, with  $Y$  and  $Z$  including the propagated uncertainties for tracer calibration, and, respectively, tracer calibration and the <sup>238</sup>U decay constant.

## 4.3. Re–Os dating

Three molybdenite separates were obtained. Two independent mineral separates were isolated using traditional mineral separation protocols – for example, crushing, magnetic Frantz separation, heavy liquids, water floatation and hand picking (Selby & Creaser 2004). The mineral separates of samples SH23A and SH23B were achieved utilising the HF isolation approach (Lawley & Selby 2012). The latter uses concentrated HF at room temperature to aid in liberating the molybdenite from the silicate matrix.

The Re–Os analytical protocol follows that described by Selby & Creaser (2001), with a slight modification to the isolation protocol of Re. An aliquot of molybdenite doped with a known amount of tracer solution comprising <sup>185</sup>Re and normal Os isotope composition was loaded into a Carius tube with a 1:3 mL mix of concentrated hydrogen chloride (HCl) and nitric acid (HNO<sub>3</sub>). The tube was sealed and then heated to 220 °C for 24 h. The Os was isolated from the acid solution using solvent extraction with chloroform and further purified using micro-distillation. The Re was isolated using solvent extraction by sodium hydroxide and acetone, and then further purified using anion HNO<sub>3</sub>:HCl chromatography.

The isotope compositions of the Re and Os fractions were determined using Negative Thermal Ionisation Mass Spectrometry (Creaser *et al.* 1991; Volkenning *et al.* 1991) using a Thermo Electron TRITON mass spectrometer at the University of Durham. Measurements were made statically using the Faraday Cups for both Re and Os. The measured Re and Os isotopic ratios were oxide-corrected offline. The data were corrected for fractionation. Analytical uncertainties are propagated and incorporate uncertainties related to Re and Os mass spectrometer measurements, blank abundances and isotopic compositions, spike calibrations and reproducibility of standard Re and Os isotope values. Procedural blanks conducted during the period of the molybdenite analysis are negligible relative to the Re and Os abundances measured in the samples (Re  $2.1 \pm 0.2$  ppt, Os  $0.1 \pm 0.2$  ppt, <sup>187</sup>Os/<sup>188</sup>Os =  $0.22 \pm 0.05$ ;  $n = 2$ ). In-house reference solutions run during the analysis (Re std =  $0.5983 \pm 0.0011$ ; DROsS =  $0.16089 \pm 0.0001$ ;  $n = 2$ ) are similar to long-term reproducibility data reported by Lawley & Selby (2012) (and references therein). The Re–Os ages are presented as model ages from the simplified isotope equation [ $t = \ln(^{187}\text{Os}/^{187}\text{Re} + 1) / \lambda$ ] (where  $t$  = model age and  $\lambda$  = <sup>187</sup>Re decay constant), and assumes no initial radiogenic Os. The inclusion of decay-constant uncertainty and reporting of data with 2-sigma uncertainty allows for direct comparison of the Re–Os ages with the <sup>206</sup>Pb/<sup>238</sup>U and <sup>40</sup>Ar/<sup>39</sup>Ar

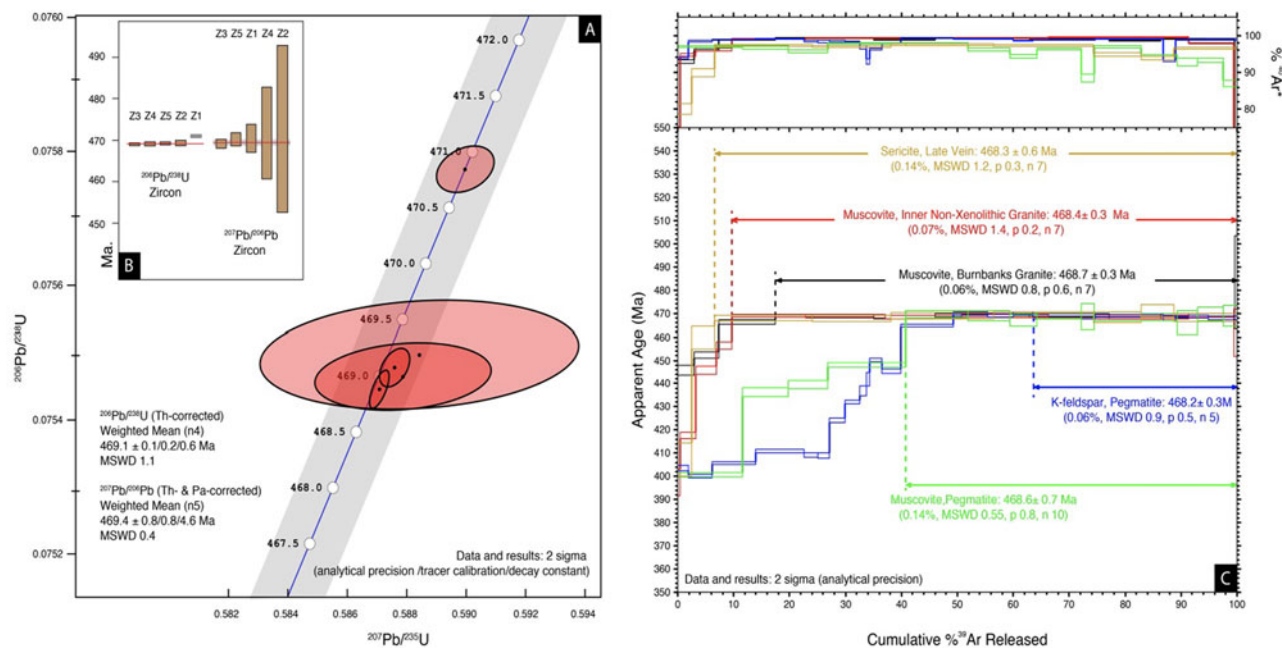


**Figure 5** (A) Zircon U–Pb Concordia plot. (B) Zircon U–Pb weighted average ages. (C)  $^{40}\text{Ar}/^{39}\text{Ar}$  step-heating spectra showing ages for all targeted samples.

ages. The Re–Os ages are provided as  $X \pm Y/Z$ , with  $Y$  and  $Z$  with and without the decay-constant uncertainty, respectively.

Appendix DM2 contains raw age data. Note, all age data throughout are reported at the 2-sigma confidence level. Also, all published data have been recalculated (where relevant) to the latest decay constants and monitor ages/spike calibrations.

## 5. Results

### 5.1. Inter-chronometer comparison

It is important to note that when considering the relative timing of different units using a single chronometer, only the analytical uncertainty is required, as mineral standard age uncertainties, tracer calibration and decay-constant uncertainties are all systematic, and have a predictable and similar effect on each sample. The age standard, tracer and decay-constant uncertainties, combined, yield the ‘total’ uncertainty and this is used when comparing data from different chronometers. All inter-chronometer comparisons throughout this contribution are made at the 2-sigma (95.4%) confidence interval and incorporate systematic uncertainties.

The weighted means (single zircon ID-TIMS) for the  $^{207}\text{Pb}/^{206}\text{Pb}$  and  $^{206}\text{Pb}/^{238}\text{U}$  ages are  $469.4 \pm 0.8/0.8/4.6$  Ma (analytical precision/tracer calibration/decay-constant uncertainties) and  $469.1 \pm 0.1/0.2/0.6$  Ma, respectively (Fig. 5). We interpret the  $^{206}\text{Pb}/^{238}\text{U}$  age to constrain crystallisation of the unfoliated non-xenolithic granite.

All  $^{40}\text{Ar}/^{39}\text{Ar}$  age spectra (Fig. 5) show, to varying degrees, a *ca.* 405 Ma disturbance of the low-temperature steps. With the exception of the K-feldspar from the pegmatite, all age spectra

step-up to define robust plateau ages. The outer Burnbanks Granite (muscovite) is  $468.7 \pm 0.3/0.4$  Ma (analytical precision/decay-constant uncertainties), the inner unfoliated non-xenolithic granite (muscovite) is  $468.4 \pm 0.3/0.4$  Ma, the pegmatite (muscovite) is  $468.6 \pm 0.7/0.7$  Ma and the late vein (muscovite) that the cuts granite, breccia and porphyry rocks is  $468.3 \pm 0.6/0.7$  Ma. The K-feldspar data step-up also from *ca.* 405 Ma to define a mini-plateau age ( $468.2 \pm 0.3/0.4$  Ma) that is indistinguishable from the age of the muscovite from the same rock. All  $^{40}\text{Ar}/^{39}\text{Ar}$  ages are indistinguishable from each other and the  $^{206}\text{Pb}/^{238}\text{U}$  zircon age. The close temporal association between the U–Pb zircon and the  $^{40}\text{Ar}/^{39}\text{Ar}$  muscovite ages shows that the SHSC, including late hydrothermal activity, was emplaced and cooled very quickly, within  $0.5 \pm 0.9$  Ma (possibly due to rapid uplift, see discussion below). The reproducible ages (*ca.* 469–468 Ma) for the outer Burnbanks granite and the SHSC, together with petrographic similarities and the symmetrical position of the outer granites on the northern and southern sides of the complex (Fig. 2), strongly suggest that they are part of the SHSC.

A molybdenite sample from the late quartz–molybdenite vein that presents as coeval with the muscovite (Fig. 4; Table 1) defines a model age of  $440.2 \pm 3.1/3.4$  Ma (analytical precision and tracer calibration/decay-constant uncertainties). Although there is excellent agreement between the  $^{40}\text{Ar}/^{39}\text{Ar}$  and U–Pb systems (Figs 5, 6), the Re–Os age is surprisingly not concordant with the other chronometers (Table 1). We do not consider the Re–Os age to be geologically robust with respect to an emplacement age (see discussion below), owing to the later alteration of the molybdenite to powellite, a mineral found in the oxidation zones of molybdenite-bearing hydrothermal deposits (Anthony *et al.* 2003).

**Table 1** Re–Os raw data and ages  $\pm$  analytical precision/full external uncertainties (lambda). The data define a weighted average age of  $438.6 \pm 1.5/1.9$  Ma.

Sample	Wt.	Re (ppm)	$\pm$	$^{187}\text{Re}$ (ppm)	$\pm$	$^{187}\text{Re}$ (ppb)	$\pm$	Age (Ma)	$\pm$	$\pm_{\text{lambda}}$
RO485-3	0.0036	20.5	0.3	12.9	0.2	94.6	1.1	440.2	3.1	3.4
RO543-2	0.0102	38.2	0.2	24.0	0.1	175.4	0.9	437.5	2.0	2.4
RO764-1	0.0085	10.1	0.1	6.3	0.1	46.8	0.4	441.9	5.3	5.5
RO764-2	0.0102	20.6	0.1	12.9	0.1	94.9	0.5	438.3	2.1	2.5

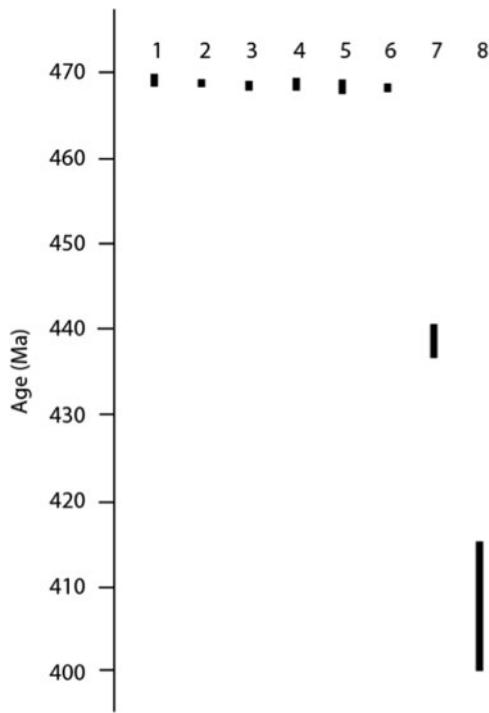


**Figure 6** Summary of multi-chronometer geochronology (all data shown at 2-sigma including all sources of uncertainties). 1:  $^{206}\text{Pb}/^{238}\text{U}$  age for zircon from the unfoliated non-xenolithic granite. 2:  $^{40}\text{Ar}/^{39}\text{Ar}$  age for the Burnbanks granite. 3:  $^{40}\text{Ar}/^{39}\text{Ar}$  age for inner unfoliated non-xenolithic granite. 4:  $^{40}\text{Ar}/^{39}\text{Ar}$  age for the pegmatite (muscovite). 5:  $^{40}\text{Ar}/^{39}\text{Ar}$  age (mini-plateau) for K-feldspar from pegmatite. 6:  $^{40}\text{Ar}/^{39}\text{Ar}$  age for the late vein. 7: Re–Os age for molybdenite from late vein. 8:  $^{40}\text{Ar}/^{39}\text{Ar}$  reset age range recorded by all  $^{40}\text{Ar}/^{39}\text{Ar}$  samples.

## 6. Discussion

### 6.1. Re–Os chronology

The young Re–Os age (Table 1; Fig. 6) was unexpected given the relatively high closure temperature ( $>500\text{ }^{\circ}\text{C}$ , certainly higher than  $^{40}\text{Ar}/^{39}\text{Ar}$  muscovite) associated with the Re–Os molybdenite system – suggesting either the molybdenite age is ‘reset’ or the molybdenite was emplaced significantly later than the SHSC. Temperatures required to thermal reset the molybdenite would have completely reset the  $^{40}\text{Ar}/^{39}\text{Ar}$  geochronometer and, as such, we would not have recovered ages for the vein muscovite equivalent to the U/Pb age of the granites. The textural evidence indicates that the molybdenite and muscovite have a close spatial association and are coeval (see Fig. 4 and discussion above). Therefore, a younger molybdenite emplacement event would require the muscovite formed coevally with the molybdenite to be younger than the granites, but the muscovite fraction dated (grainsize 50 to 100s  $\mu\text{m}$ ) is not temporally resolvable from the age of the granites. In an attempt to resolve this conundrum, we re-examined the samples by scanning electron microscopy (SEM), which revealed the presence of powellite.

Powellite (calcium molybdate) in our samples is closely associated with molybdenite, and is best developed in the clusters and, to a lesser extent, in the margin-parallel veinlets (Fig. 7). There is evidence that powellite was formed during a separate and later event to molybdenite. Thus, ragged molybdenite crystals occur floating in powellite, which also penetrates along molybdenite cleavages supporting a replacive relationship (Fig. 7b, c). Commonly, molybdenite crystals or terminations of crystals enclosed by quartz are not coated by powellite (Fig. 7a), which is consistent with quartz protecting molybdenite from alteration by later fluids. Powellite is present by itself in

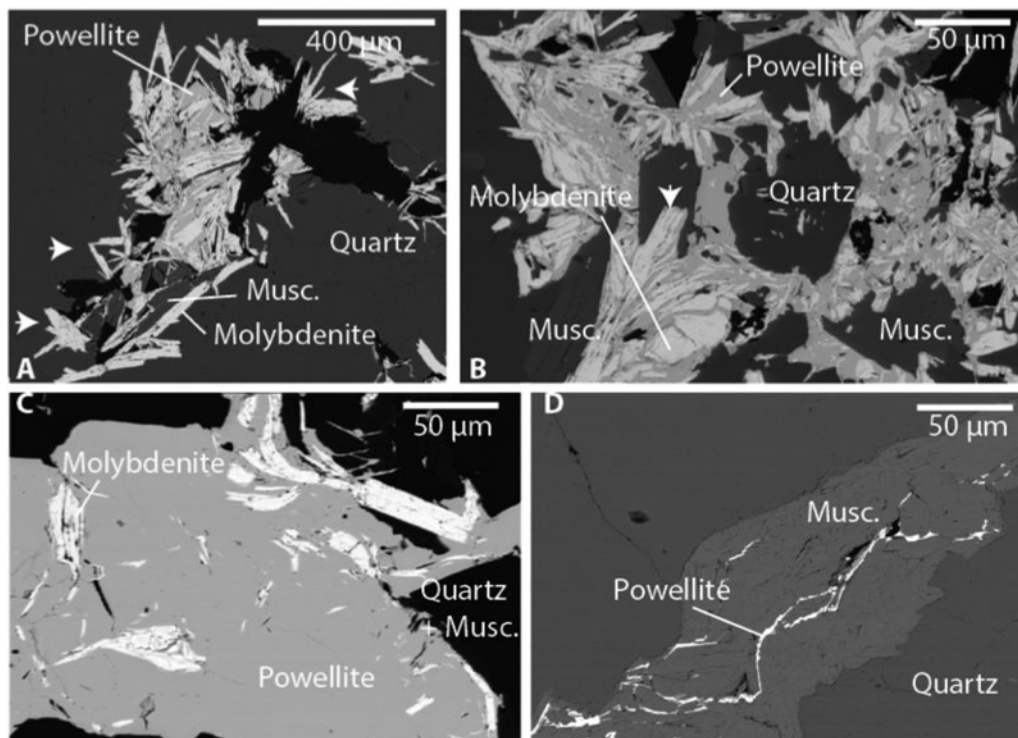


**Figure 7** (A) BSEM: molybdenite (white), minor muscovite (dark grey) and powellite (medium grey) in quartz (dark grey). Note that powellite encloses molybdenite in the cluster but not where molybdenite terminations are protected in quartz (white arrows). (B) BSEM: molybdenite (white) and powellite (medium grey) in quartz (dark grey) with minor muscovite. Powellite enclosing molybdenite crystals of varying size and ragged appearance. Note powellite penetrating along molybdenite cleavages (white arrow). (C) BSEM: powellite (medium grey) is enclosing ragged molybdenite crystals. (D) BSEM: powellite filling fine fractures in muscovite.



fracture fills in muscovite (Fig. 7d). Further petrographic evidence for a later tectono-hydrothermal event, possibly linked to powellite deposition, are margin-parallel bright-quartz veinlets and fracture-controlled inclusion trails cutting the dark-quartz network (Fig. 4b).

Therefore, we propose an alternate scenario, which suggests caution must be employed if using the Re–Os molybdenite-dating tool (model ages) in isolation of other chronometers in settings that have experienced multiple magmatic and hydrothermal events. The alteration of molybdenite to powellite has resulted in (owing to bulk dissolution/sampling approaches) a two-component hybrid age that has no geological significance. This is supported by the  $^{40}\text{Ar}/^{39}\text{Ar}$  step-heating data recording an alteration/fluid flushing event at *ca.*405 Ma (Figs 5, 6), which is likely linked to the emplacement of the nearby Mt Battock granite of equivalent age (Oliver *et al.* 2008). Hydrothermally driven fluid flushing events (e.g., Mark *et al.* 2007) likely formed the powellite whilst also disturbing the Ar-systematics of the low closure temperature minerals (e.g., feldspar), producing the 405 Ma overprint. The primary molybdenite age (*ca.*468 Ma) mixed in the correct portions with a younger powellite age (*ca.*405 Ma), would yield a 438–441 Ma hybrid age. Note, there is no known thermal event that is coincident with the *ca.*440 Ma model Re–Os age in the area of study.

Although powellite has been found in other systems, a disturbance of the Re–Os ages has not been reported, which is likely because the powellite formed soon after molybdenite deposition; thus, the molybdenite age uncertainties would mask any disturbances to the Re–Os system (the delta-time between the molybdenite and powellite is small, whereas, at Souter Head, the delta-time between the molybdenite formation and subsequent powellite formation is large). The powellite at Souter Head formed much later than the molybdenite, beyond the uncertainties of the molybdenite Re–Os age as suggested by the young (*ca.*405 Ma)  $^{40}\text{Ar}/^{39}\text{Ar}$  age. Several studies have conducted experiments to establish the effect of such alteration on the Re–Os chronometer (e.g., Suzuki *et al.* 2000), with much discussion and debate (e.g., Selby *et al.* 2004; Suzuki 2004). Suzuki *et al.* (2000) showed experimentally that the Re–Os system in molybdenite can behave as an open-system in the presence of aggressive advecting fluids.

## 6.2. The age of the SHSC

The ages obtained for the SHSC show that it belongs to the Ordovician late tectonic granites (*ca.*475–457 Ma) of the NE Grampian Terrane (Strachan *et al.* 2002; Oliver *et al.* 2008) rather than the Silurian–Devonian newer granites (Fig. 8). The former are mostly S-type two-mica granites, garnet-bearing and commonly foliated with strontium-87 ( $^{87}\text{Sr}$ )/ $^{86}\text{Sr}$  ratios consistent with the melting of sedimentary protoliths (Chappell & White 1974; Harmon 1983). Infracrustal sources may also be involved (Appleby *et al.* 2010).

Stages of deformation associated with the Grampian Event in NE Scotland are D1–D3 and, locally, D4 (Harte *et al.* 1984; Kneller 1987; Strachan *et al.* 2002). The SHSC intrudes the Barrovian metamorphic core (sillimanite zone) in this area (Fig. 1c) where peak metamorphism is closely associated with D3 (Harte *et al.* 1984; McClellan 1989). The nearby-foliated Aberdeen granite is broadly D3 and has been dated at  $470 \pm 2$  Ma (Kneller & Aftalion 1987) (Fig. 1d). The SHSC is similar in terms of mineralogy to these granites but, critically, lacks a tectonic foliation. The geochronology, absence of a tectonic foliation and widespread evidence of brittle rather than ductile deformation in the SHSC, as well as the absence of high-grade indicator minerals and significant recrystallisation, shows the SHSC immediately post-dates and, thus, constrains the end of

main (D1–D3) Grampian deformation and metamorphism in the NE Grampian terrane to  $469.1 \pm 0.6$  Ma.

## 6.3. Termination and duration of the Grampian Event

The post-deformation SHSC age is indistinguishable from garnet Sm–Nd ages that place the end of D3 at Glen Clova at  $466.8 \pm 3.2$  Ma (2-sigma, full external uncertainties; Baxter *et al.* 2002) (Fig. 1b). Similarly, the SHSC age is coincident with the termination of deformation to the N at Portsoy, as constrained by an undeformed pegmatite at  $474 \pm 5$  Ma (Carty *et al.* 2012).

Given that the ages for the SHSC, Glen Clova and Portsoy are indistinguishable at the 2-sigma confidence interval, we have calculated a weighted average of the termination of D3 deformation and peak metamorphism in NE Scotland of  $469.2 \pm 1.3$  Ma. Thus, the duration of the Grampian Event at best can be confined to  $22.8 \pm 2.4$  Ma, from the onset of collision (i.e., ophiolite obduction) to the termination of Grampian Event D3 deformation. A later phase of deformation D4 is developed locally N of the HBF, but the age of this event is currently unconstrained. It has been linked to late-stage uplift of the orogen (Harte *et al.* 1984).

## 6.4. Termination and rapid uplift

There is direct evidence that rapid uplift was temporally associated with the termination of the orogenic peak in NE Scotland. The SHSC was emplaced in sillimanite zone rocks in the upper crust (above *ca.*10 km) as demonstrated by the presence of porphyritic rocks and widespread evidence of brittle fracture – that is, intrusive breccias with angular clasts and parallel-sided quartz and pegmatite veins (Seedorf *et al.* 2005).

A further estimate of depth was obtained using the normative quartz and albite plus orthoclase barometers (Yang 2017). We applied this method to four granitic members of the Souter Head suite to constrain the depth (Appendix DM3). Three of them were at the extreme limits of the calibration of the method and the results should be treated with caution. However, a quartz–feldspar porphyry falls well within the range of the calibration method and yields a depth estimate of 13–15 km. Overall, an emplacement depth in the range 10–15 km for the SHSC is indicated.

However,  $0.9 \pm 2$  Ma prior to emplacement of the SHSC, as evidenced by the nearby foliated (syn-D3) Aberdeen Granite ( $470 \pm 2$  Ma), the host rocks of the SHSC were in the lower crust at *ca.*20 km depth (Vorhies & Ague 2011), experiencing high-grade metamorphism under ductile conditions. Within a short time period, these rocks thus underwent a 5–10 km change in their structural level – requiring an exhumation rate of  $5\text{--}10 \text{ km Ma}^{-1}$ , comparable to rates found in modern arc-continent collision zones (Brown *et al.* 2011).

By *ca.*469 Ma, much of the metamorphic cover was removed, which is consistent with high-grade orogenic debris arriving in the South Mayo Trough, Connemara and Midland Valley Basin (Kirkland Conglomerate) at  $465 \pm 3$  Ma and with the oldest mica (Dalradian and detrital) cooling ages (Oliver *et al.* 2000; Oliver 2001; Clift *et al.* 2004; Dewey 2005). The lag time for sediment transport to the Midland Valley basin was exceptionally short, potentially 0.1 Ma, allowing for the large uncertainty associated with the lower (*ca.*465 Ma) bound for the Kirkland Conglomerate. These data support our age for exhumation of the metamorphic core.

## 6.5. Slab break-off and timing of events during the metamorphic peak

The Grampian orogenic peak is defined by temporally overlapping D2/D3 deformation and peak metamorphism, basic

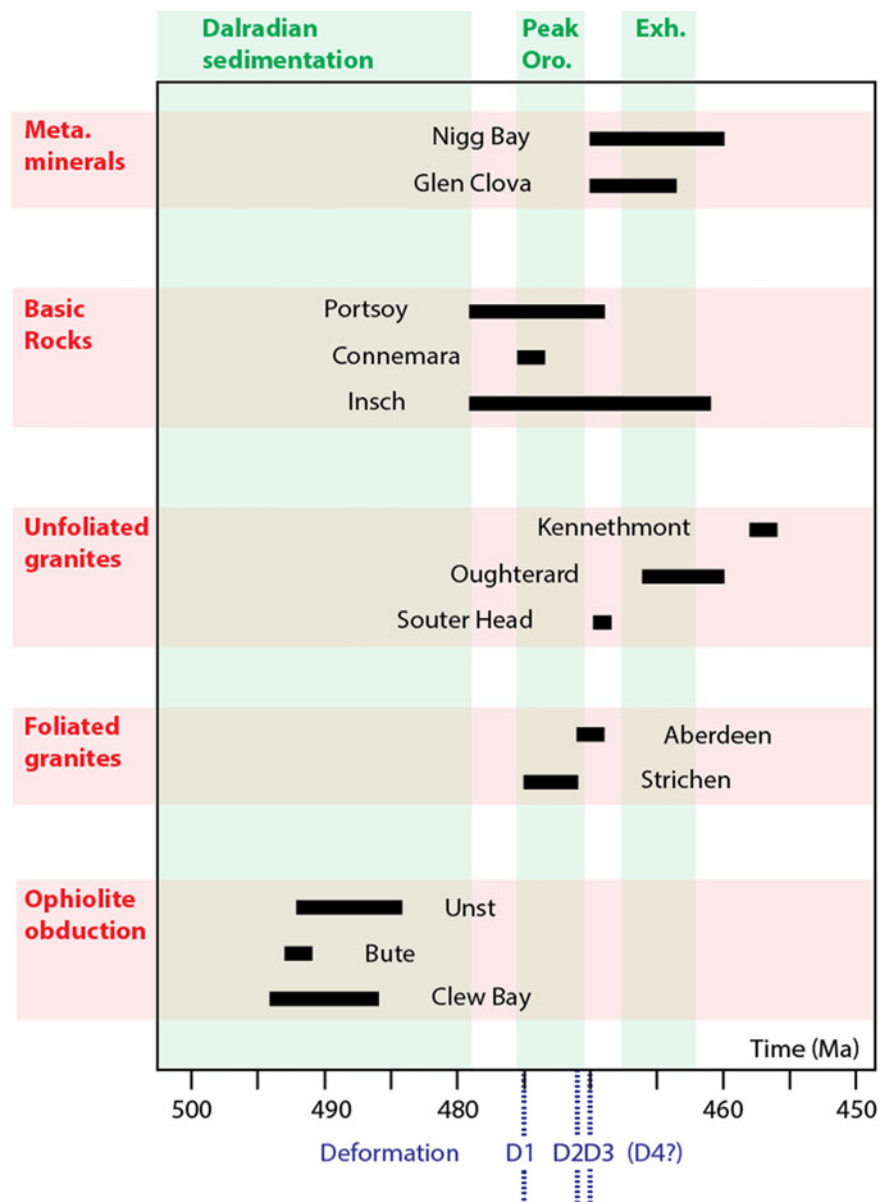


**Figure 8** Timescale showing the age of key metamorphic (meta.) minerals, basic rocks, unfoliated granites, foliated granites and ophiolite obduction in NE Scotland and western Ireland in relation to Dalradian sedimentation, peak orogenesis (oro.) and exhumation (exh.). Data from Baxter *et al.* (2002), Carty *et al.* (2012), Chew *et al.* (2010), Dempster *et al.* (2002), Friedrich *et al.* (1999), Kneller & Aftalion (1987), Oliver *et al.* (2000), Stewart *et al.* (2017) and Viète *et al.* (2013). The various times of deformation (D1–D4) are also shown.

magmatism and rapid uplift all within *ca.* 5 Ma, which points towards a critical and abrupt change in the subduction zone (Fig. 9). Through comparison with numerical simulations (see below), this is best explained by slab break-off, which likely occurred soon after buoyant material (a spreading ridge or the Midland Valley Arc) entered the trench and stalled subduction (Oliver *et al.* 2008; Tanner 2014). Although slab roll-back, slab tearing or slab-parallel asthenospheric melting are other potential explanations, numerical simulations suggest none of these mechanisms are congruent with an abrupt event that results in a structural change of 5–10 km within the crust within  $0.9 \pm 2$  Ma (Menant *et al.* 2016; Cassel *et al.* 2018 and references within).

When slab break-off occurs, part of a subducted lithospheric plate detaches abruptly and sinks into the asthenosphere, inducing upwelling. The dynamics of slab break-off have been investigated extensively, and it has been shown that the strength of the subducting lithosphere, in part influenced by the oceanic slab age, convergence velocity, continental crustal and lithospheric thicknesses, and the mechanism of detachment, all exert control

on the depth of break-off (Gerya *et al.* 2004; Andrews & Billen 2009; Duretz *et al.* 2011). Numerical models have shown a wide range in this depth, from 40 to over 500 km (Baumann *et al.* 2010; Duretz *et al.* 2011), but few numerical modelling studies have quantitatively examined the topographic response (rate and amount of uplift) to slab detachment. For example, Buiter *et al.* (2002) predicted topography uplift in the range of 2–6 km using an elastic model, whereas Gerya *et al.* (2004) predicted lower uplift values (<2 km) using a visco-plastic model. Analysis of ancient orogenic belts – for example, the Grampian Event – provides a time-integrated picture of topographic evolution (as opposed to modern-day measurements in active subduction zones) that allows for connection between model and real-world data.

Some 5–10 km of uplift as recorded by the SHSC over *ca.* 1 Ma would suggest a slab break-off depth of either less than 100 km (Buiter *et al.* 2002) or less than 50 km (Duretz *et al.* 2011). Slab break-off at *ca.* 50 km depth would be directly under the collision zone. We suggest that the ensuing rapid uplift caused

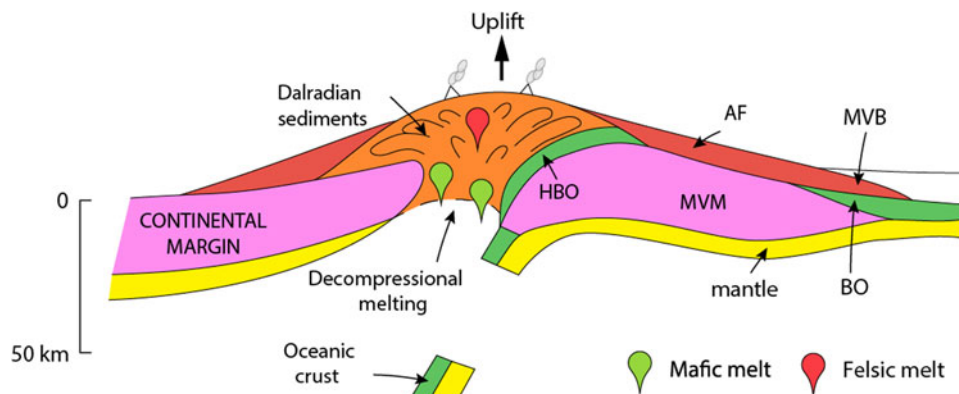


**Figure 9** Cross-section of the Grampian Orogen in NE Scotland during and immediately after slab break-off *ca.* 471 Ma (Portsoy). The orogen is undergoing rapid uplift and exhumation. Crustal thinning through erosion and detachment faulting (not shown, see text) as the orogen collapses promotes decompressional melting to produce mafic and felsic melts. The figure is influenced by Oliver *et al.* (2008) and Tanner (2014). Abbreviations: AF = Alluvial fan; BO = Ballantrae ophiolite; HBO = Highland Border ophiolite; MVB = Midland Valley basin; MVM = Midland Valley microcontinent.

crustal thinning and decompressional melting of the subcrustal mantle (McKenzie & Bickle 1989; Hole *et al.* 2015). This depth is consistent with the shallow sourcing of basic melts to power Buchan metamorphism in NE Scotland (and Ireland, see below) (Viète *et al.* 2013, 2017; Johnson *et al.* 2017). Crustal thinning could be achieved by erosion and gravity-driven detachment faulting, as suggested for Connemara where the uplift rate is similar (Clift *et al.* 2004). Melting of the lower crust may also have occurred by decompression/invasion by basic magma to produce the syn- and post-D3 granites observed throughout the region (e.g., the Aberdeen granite and the SHSC).

The precise age of slab break-off during the Grampian Event is uncertain but can be constrained by the age of basic magmatism. The oldest known and precisely dated synorogenic basic rock in NE Scotland is  $471.3 \pm 1.7$  Ma (Carty *et al.* 2012) and, in Connemara,  $ca. 474.5 \pm 1$  Ma (Friedrich *et al.* 1999). Rapid uplift likely began no later than 470 Ma and may have occurred along regional shear zones such as the Portsoy Shear Zone, which also controlled magma emplacement (Ashcroft *et al.* 1984; Carty *et al.* 2012; Viète *et al.* 2013). Meanwhile, orogenic detritus accumulated in adjacent sedimentary basins (Dewey & Mange 1999; Oliver 2001).

These observations suggest that a switch from compressional to extensional tectonics in the orogen occurred in the period 474–471 Ma and overlaps with peak Barrovian and Buchan metamorphism and D2/D3 deformation. While we agree with Viète *et al.* (2013) that regional extension was the likely tectonic setting for peak metamorphism and deformation, we consider that slab break-off (Oliver *et al.* 2008; Tanner 2014) provides a better model to explain the extensional processes involved in this very short event.

### 6.6. Scotland and Connemara

There are marked similarities in the timings and rates of specific events in NE Scotland with Connemara in western Ireland: peak metamorphism and deformation terminated at *ca.* 470–468 Ma (Friedrich *et al.* 1999); uplift rates at the termination of the orogeny in Connemara were *ca.* 7 km Ma<sup>-1</sup> (Friedrich & Hodges 2016); and these events are essentially coincident with intrusion of basic syn-D3 plutons (e.g., Cashel-Lough Wheelaun gabbro,  $470.1 \pm 1.4$  Ma; Friedrich *et al.* 1999). Such data suggest that shallow slab detachment occurred synchronously in NE Scotland and Connemara. Along-strike heterogeneity in subduction zones is well known (e.g., Nazca Plate; Chen *et al.* 2001; Brown *et al.* 2011 and references therein) and it is likely that slab detachment did not occur in the intervening portion of the subduction

zone where Barrovian metamorphism only is found. Here, slab dips were mainly shallow and, consequently, with the exception of the Tyrone Igneous Complex, arc-related igneous activity was essentially absent (Fig. 1b) (Cahill & Isacks 1992; Chen *et al.* 2001; Cooper *et al.* 2011).

## 7. Conclusions

The SHSC (Aberdeenshire, Scotland) intruded the high-grade metamorphic core of the Grampian Orogen at  $469.1 \pm 0.6$  Ma (<sup>238</sup>U–<sup>206</sup>Pb zircon). Temporally coincident U–Pb and <sup>40</sup>Ar/<sup>39</sup>Ar data show the SHSC cooled quickly. Intrusion followed closely peak metamorphism and D2/D3 deformation at *ca.* 470 Ma and marks the end of the Grampian Event in NE Scotland. Younger Re–Os ages are due to post-emplacment alteration of molybdenite to powellite and highlight the importance of careful petrographic characterisation of materials prior to determination of model Re–Os ages from molybdenite.

D2/D3 Grampian deformation (the age of D1 remains uncertain), peak metamorphism (Barrovian and Buchan style) and basic magmatism in NE Scotland were synchronous at *ca.* 470 Ma and associated with rapid uplift (5–10 km Ma<sup>-1</sup>) of the orogen, which largely removed the metamorphic cover by *ca.* 469 Ma. We suggest that shallow slab break-off (50–100 km) can explain the rapid uplift and the synchronicity of these events, and that decompression led to melting and generation of mafic and felsic melts. This interpretation implies that peak metamorphism and D2/D3 ductile deformation were associated with extension, as previously suggested. Close similarities between the geological histories of NE Scotland and Connemara suggest that shallow slab break-off occurred in both areas. Our proposed model explains the presence of both Buchan and Barrovian metamorphism in certain sectors.

## 8. Supplementary material

Supplementary material is available online at <https://doi.org/10.1017/S1755691020000043>.

## 9. Acknowledgements

Scottish Universities Environmental Research Centre (SUERC) would like to thank NERC for continued funding of the NERC Argon Isotope Facility. We would like to thank the following: Joyce Neilson/Natalie Farrell, John Still, Jenny Johnston/Jamie Bowie and the Lyon Bequest (University of Aberdeen) for

discussion of CL data, assistance with the SEM, preparing figures and funding the work, respectively. Ross Dymock and Jim Imlach (SUERC) are thanked for their assistance with sample preparation. Martin Lee at the School of Geographical and Earth Sciences at the University of Glasgow for use of the SEM/CL equipment and Peter Chung for technical assistance. David Selby at the University of Durham for the Re–Os analyses and discussion of the data.

## 10. References

- Ague, J. J. & Baxter, E. F. 2007. Brief thermal pulses during mountain building recorded by Sr diffusion in apatite and multicomponent diffusion in garnet. *Earth & Planetary Science Letters* **261**, 500–16.
- Andrews, E. R. & Billen, M. I. 2009. Rheologic controls on the dynamics of slab detachment. *Tectonophysics* **464**, 60–69.
- Anthony, J. W., Bideaux, R. A., Bladh, K. W. & Nichols, M. C. 2003. *Handbook of mineralogy*, 5, Tucson, Arizona: Mineral Data Publishing, 813 pp.
- Appleby, S. K., Gillespie, M. R., Graham, C. M., Hinton, R. W., Oliver, G. J. H. & Kelly, N. M. 2010. Do S-type granites commonly sample infracrustal sources? New results from an integrated O, U–Pb and Hf isotope study of zircon. *Contributions Mineralogy and Petrology* **160**, 115–32.
- Ashcroft, W. A., Kneller, B., Leslie, A. G. & Munro, M. 1984. Major shear zones and autochthonous Dalradian in the northeast Scottish Caledonides. *Nature, London* **310**, 760–62.
- Barfod, D. N., Mark, D. F., Tait, A., Dymock, R. C. & Imlach, J. 2014. Argon extraction from geological samples by CO<sub>2</sub> scanning laser step-heating. *Geological Society Special Publication* **378**, 79–90.
- Baumann, C., Gerya, T. V. & Connolly, A. D. 2010. Numerical modelling of spontaneous slab breakoff dynamics during continent collision. *Geological Society, London, Special Publications* **332**, 99–114, 1.
- Baxter, E. F., Ague, J. J. & Depaulo, D. J. 2002. Prograde temperature–time evolution in the Barrovian type-locality constrained by Sm/Nd garnet ages from Glen Clova, Scotland. *Journal Geological Society, London* **159**, 71–82.
- Bowring, J. F. & Mclean, N. M. 2011. Engineering cyber infrastructure for U–Pb geochronology: Tripoli and U–Pb\_Redux. *Geochemical Geophysics Geosystems* **12**, Q0AA19.
- Brown, D., Ryan, P. D., Afonso, J. C., Boutelier, D., Burg, J. P., Byrne, T., Calvert, A., Cook, F., DeBari, S., Dewey, J. F., Gerya, T. V., Harris, R., Herrington, R., Konstantinovskaya, E., Reston, T. & Zagorevski, A. 2011. Arc-Continent collision: the making of an orogen. In Brown, D. & Ryan, P. (eds) *Arc-continent collision, frontiers in earth science*, 477–93. Heidelberg: Springer, Springer-Verlag.
- Buiter, S. J. H., Govers, R. & Wortel, M. J. R. 2002. Two-dimensional simulation of surface deformation caused by slab detachment. *Tectonophysics* **354**, 195–210. [https://link.springer.com/chapter/10.1007/978-3-540-88558-0\\_17](https://link.springer.com/chapter/10.1007/978-3-540-88558-0_17)
- Cahill, T. & Isacks, B. L. 1992. Seismicity and shape of the subducted Nazca Plate. *Journal of Geophysical Research* **97**, 503–17, 529.
- Carty, J. P., Connelly, J. N., Hudson, N. F. C. & Gale, J. F. W. 2012. Constraints on the timing of deformation, magmatism and metamorphism in the Dalradian of NE Scotland. *Journal Geological Society, London* **48**, 103–07.
- Cassel, E. J., Smith, M. E. & Jicha, B. R. 2018. The impact of slab rollback on Earth's surface: uplift and extension in the hinterland of the North American Cordillera. *Geophysical Research Letters* **45**, 10996–1004.
- Chappell, B. W. & White, A. J. R. 1974. Two contrasting granite types. *Pacific Geology* **8**, 173–74.
- Chen, P. F., Bina, C. R. & Okal, E. A. 2001. Variations in slab dip along the subducting Nazca Plate as related to stress patterns and moment release of intermediate-depth seismicity and to surface volcanism. *Geochemistry, Geophysics, Geosystems* **2**. <https://agupubs.onlinelibrary.wiley.com/doi/full/10.1029/2001GC000153>
- Chew, D. M., Daly, J. S., Magna, T., Page, L. M., Kirkland, C. L., Whitehouse, M. J. & Lam, R. 2010. Timing of ophiolite obduction in the Grampian orogen. *GSA Bulletin* **122**, 1787–99.
- Chew, D. M. & Strachan, R. A. 2013. The Laurentian Caledonides of Scotland and Ireland. In Corfu, F., Gasser, D. & Chew, D. M. (eds) *New perspectives on the Caledonides of Scandinavia and related areas*, 390, 45–91. Geological Society, London, Special Publication. <https://sp.lyellcollection.org/content/390/1/45>
- Clift, P. D., Dewey, J. F., Draut, A. E., Chew, D. M., Mange, M. & Ryan, P. D. 2004. Rapid tectonic exhumation, detachment faulting and orogenic collapse in the Caledonides of western Ireland. *Tectonophysics* **384**, 91–113.
- Condon, D. J., Schoene, B. & Mclean, N. M. 2015. Metrology and traceability of U–Pb isotope dilution geochronology (EARTHTIME Tracer Calibration Part I). *Geochimica et Cosmochimica Acta* **164**, 464–80.
- Cooper, M. R., Crowley, Q. C., Hollis, S. P., Noble, S. R., Roberts, S., Chew, D., Earls, G., Herrington, R. & Merriman, R. J. 2011. Age constraints and geochemistry of the Ordovician Tyrone Igneous Complex, northern Ireland: implications for the Grampian orogeny. *Journal Geological Society, London* **168**, 837–50.
- Creaser, R. A., Papanastassiou, D. A. & Wasserburg, G. J. 1991. Negative thermal ion mass spectrometry of osmium, rhenium and iridium. *Geochimica et Cosmochimica Acta* **55**, 397–401.
- Crowley, Q. G. & Strachan, R. A. 2015. U–Pb zircon constraints on obduction initiation of the Unst Ophiolite: an oceanic core complex in the Scottish Caledonides? *Journal of the Geological Society, London* **172**, 279–82.
- Dempster, T. J., Rogers, G., Tanner, P. W. G., Bluck, M. J., Redwood, R. J., Ireland, T. R. & Paterson, B. A. 2002. Timing and deposition, orogenesis and glaciation within the Dalradian rocks of Scotland: constraints from U–Pb ages. *Journal Geological Society, London* **159**, 83–94.
- Dewey, J. & Mange, M. 1999. Petrography of Ordovician and Silurian sediments in the western Ireland Caledonides: traces of a short-lived Ordovician continent–arc collision orogeny and the evolution of the Laurentian Appalachian–Caledonide margin. In Macniocail, C. & Ryan, P. D. (eds) *Continental tectonics*, 164, 55–107. Geological Society, London. Special Publications. <https://sp.lyellcollection.org/content/164/1/55>
- Dewey, J. F. 2005. Orogeny can be very short. *Proceedings of the National Academy of Sciences* **102**, 15286–93.
- Duret, T., Gerva, T. V. & May, D. A. 2011. Numerical modelling of spontaneous slab breakoff and subsequent topographic response. *Tectonophysics* **502**, 244–56.
- Friedrich, A. M., Hodges, K. V., Bowring, S. A. & Martin, M. W. 1999. Geochronological constraints on the magmatic, metamorphic and thermal evolution of the Connemara, Caledonides, western Ireland. *Journal Geological Society of London* **156**, 1217–30.
- Friedrich, A. M. & Hodges, K. V. 2016. Geological significance of 40Ar/39Ar mica ages across a mid-crustal continental plate margin, Connemara (Grampian Orogeny, Irish Caledonides), implications for the evolution of lithospheric collisions. *Canadian Journal of Earth Sciences* **53**, 1258–78.
- Gerya, T. D., Yuen, D. A. & Maresch, W. V. 2004. Thermomechanical modelling of slab detachment. *Earth & Planetary Science Letters* **226**, 101–16.
- Harmon, R. S. 1983. Oxygen and strontium isotope evidence regarding the role of continental crust in the origin and evolution of the British Caledonian granites. In Atherton, M. P. & Gribble, C. D. (eds) *Migmatites, melting and metamorphism*, 62–79. Shiva, Orpington. <https://pascal-francis.inist.fr/vibad/index.php?action=getRecordDetail&idt=7314189>
- Harte, B., Booth, J. E., Dempster, T. J., Fettes, D. J., Mendum, J. R. & Watts, D. 1984. Aspects of the post-depositional evolution of Dalradian and Highland Border Complex rocks in the Southern Highlands of Scotland. *Transactions of the Royal Society of Edinburgh: Earth Sciences* **75**, 151–63.
- Harte, B., Booth, J. E. & Fettes, D. J. 1987. Stonehaven to Findon: Dalradian structures and metamorphism. In Trewin, N. H., Kneller, B. C. & Gillen, C. (eds) *Geology of the Aberdeen area*, 211–26. Geological Society of Aberdeen. Scottish Academic Press. <https://abdn.pure.elsevier.com/en/publications/excursion-guide-to-the-geology-of-the-aberdeen-area-scotland>
- Hole, M. J., Millett, J. M., Rogers, N. W. & Jolley, D. W. 2015. Rifting and mafic magmatism in the Hebridean basins. *Journal of the Geological Society, London* **172**, 218–36.
- Ickert, R. B., Mundil, R., Magee, Jr., C. W. & Mulcahy, S. R. 2015. The U–Th–Pb systematics of zircon from the Bishop Tuff: a case study in challenges to high precision Pb/U geochronology at millennial scale. *Geochimica et Cosmochimica Acta* **168**, 88–110.
- Johnson, T. E., Kirkland, C. L., Viète, D. R., Fischer, S., Reddy, S. M., Evans, N. J. & McDonald, B. J. 2017. Zircon geochronology reveals polyphase magmatism and crustal anatexis in the Buchan Block, NE Scotland: implications for the Grampian Orogeny. *Geoscience Frontiers* **8**, 1469–78.
- Kneller, B. C. 1987. A geological history of north-east Scotland. In Trewin, N. H., Kneller, B. C. & Gillen, C. (eds) *Geology of the Aberdeen area*, 1–50. Geological Society of Aberdeen. Scottish Academic Press. <https://abdn.pure.elsevier.com/en/publications/excursion-guide-to-the-geology-of-the-aberdeen-area-scotland>

- Kneller, B. C. & Aftalion, M. 1987. The isotopic and structural age of the Aberdeen granite. *Journal Geological Society of London* **144**, 717–22.
- Kneller, B. C. & Gillen, C. 1987. Aberdeen city and environs, excursion 1. In Trewin, N. H., Kneller, B. C. & Gillen, C. (eds) *Geology of the Aberdeen area*, 55–64. Geological Society of Aberdeen. Scottish Academic Press. <https://abdn.pure.elsevier.com/en/publications/excursion-guide-to-the-geology-of-the-aberdeen-area-scotland>
- Lawley, C. J. M. & Selby, D. 2012. Re-Os Geochronology of Quartz Enclosed ultrafine Molybdenite: Implications for Ore Geochronology. *Economic Geology* **107**, 1499–506.
- Lee, J.-Y., Marti, K., Severinghaus, J. P., Kawamura, K., Yoo, H. S., Lee, J. B. & Kim, J. S. 2006. A redetermination of the isotopic abundances of atmospheric Ar. *Geochimica et Cosmochimica Acta* **70**, 4507–12.
- Mackie, W. 1926. The heavier accessory minerals in the granites of Scotland. *Transactions of the Edinburgh Geological Society* **12**, 22–40.
- Mark, D. F., Parnell, J., Kelley, S. P., Lee, M., Sherlock, S. C. & Carr, A. 2005. Dating of multistage fluid flow in sandstones. *Science (New York, N.Y.)* **309**, 2048–51.
- Mark, D. F., Parnell, J., Kelley, S. P. & Sherlock, S. C. 2007. Resolution of regional fluid flow related to successive orogenic events on the Laurentian margin. *Geology* **35**, 547–50.
- Mark, D. F., Barfod, D. N., Stuart, F. M. & Imlach, J. G. 2009. The ARGUS multicollector noble gas mass spectrometer: performance for  $^{40}\text{Ar}/^{39}\text{Ar}$  geochronology. *Geophysics Geochemistry Geosystems* **10**, 1–9.
- Mark, D. F., Stuart, F. M. & De PODESTA, M. 2011. New high-precision measurements of the isotopic composition of atmospheric argon. *Geochimica et Cosmochimica Acta* **75**, 7494–501.
- Mark, D. F., Renne, P. R., Dymock, R., Smith, V. C., Simon, J. I., Morgan, L. E., Staff, R. A. & Ellis, B. S. 2017. High precision Ar/Ar dating of Pleistocene tuffs and temporal anchoring of the Matuyama-Brunhes boundary. *Quaternary Geochronology* **39**, 1–23.
- Mattinson, J. M. 2005. Zircon U-Pb chemical abrasion ('CA-TIMS') method: Combined annealing and multi-step partial dissolution analysis for improved precision and accuracy of zircon ages. *Chemical Geology* **220**, 47–66.
- Mckenzie, D. P. & Bickle, M. J. 1989. The volume and composition of melt generated by extension of the lithosphere. *Journal of Petrology* **29**, 625–79.
- Mckerrrow, W. S. & Campbell, C. J. 1960. The stratigraphy and structure of the lower Palaeozoic rocks of north-west Galway. *Proceedings of the Royal Society of Dublin* **1**, 27–52.
- McLean, N., Bowring, J. F. & Bowring, S. A. 2011. An algorithm for U-Pb isotope dilution data reduction and uncertainty propagation. *Geochemistry Geophysics Geosystems* **12**, Q0AA18.
- McClellan, E. L. 1985. Metamorphic reactions in the kyanite and sillimanite zones of the Barrovian type area. *Journal of Petrology* **26**, 789–818.
- McClellan, E. L. 1989. Sequential formation of subsolidus and anatectic migmatites in response to thermal evolution, eastern Scotland. *Journal of Geology* **97**, 165–82.
- Menant, A., Sternai, P., Jolivet, L., Guillou-Frottier, L. & Gerya, T. 2016. 3D Numerical modeling of mantle flow, crustal dynamics and magma genesis associated with slab roll-back and tearing: The eastern Mediterranean case. *Earth and Planetary Science Letters* **442**, 93–107.
- Morgan, L. E., Mark, D. F., Imlach, J., Barfod, D. & Dymock, R. 2014. FCs-EK: a new sampling of the Fish Canyon Tuff  $^{40}\text{Ar}/^{39}\text{Ar}$  neutron flux monitor. *Geological Society Special Publication* **378**, 63–67.
- Munro, M. 1986. Geology of the country around Aberdeen. Memoir of the British Geological Survey, Sheet 77 (Scotland).
- Noble, S. R., Condon, D. J., Carney, J. N., Wilby, P. R., Pharaoh, T. C. & Ford, T. D. 2014. U-Pb geochronology and global context of the Charnian Supergroup, UK: Constraints on the age of key Ediacaran fossil assemblages. *Geological Society of America Bulletin* **127**, 250–65.
- Oliver, G. J. H. 2001. Reconstruction of the Grampian episode in Scotland; its place in the Caledonian Orogeny. *Tectonophysics* **332**, 23–49.
- Oliver, G. J. H., Chen, F., Buchwaldt, R. & Hegner, E. 2000. Fast tectonometamorphism and exhumation in the type area of the Barrovian and Buchan zones. *Geology* **28**, 459–62.
- Oliver, G. J. H., Wilde, S. A. & Wan, Y. 2008. Geochronology and geodynamics of Scottish granulites from the late Neoproterozoic break-up of Rodinia to Palaeozoic collision. *Journal Geological Society of London* **165**, 661–74.
- Paterson, S. R., Vernon, R. H. & Tobisch, O. T. 1989. A review of criteria for the identification of magmatic and tectonic foliations in granulites. *Journal of Structural Geology* **11**, 349–63.
- Porteous, W. G. 1973. A breccia pipe in the Dalradian series, East Kincardineshire. *Scottish Journal Geology* **9**, 233–37.
- Renne, P. R., Cassata, W. S. & Morgan, L. E. 2009. The isotopic composition of atmospheric argon and  $^{40}\text{Ar}/^{39}\text{Ar}$  geochronology: time for a change? *Quaternary Geochronology* **4**, 288–98.
- Renne, P. R., Mundil, R., Balco, G., Min, K. & Ludwig, K. R. 2010. Joint determination of 40 K decay constants and  $^{40}\text{Ar}/^{40}\text{K}$  for the Fish Canyon sanidine standard, and improved accuracy for  $^{40}\text{Ar}/^{39}\text{Ar}$  geochronology. *Geochimica et Cosmochimica Acta* **74**, 5349–67.
- Renne, P. R., Balco, G., Ludwig, K. R., Mundil, R. & Min, K. 2011. Response to the comment by W.H. Schwarz et al. On 'Joint determination of 40 K decay constants and  $^{40}\text{Ar}/^{40}\text{K}$  for the Fish Canyon sanidine standard, and improved accuracy for  $^{40}\text{Ar}/^{39}\text{Ar}$  geochronology' by P.R. Renne et al. (2010). *Geochimica et Cosmochimica Acta* **75**, 5097–100.
- Rice, C. & Mark, D. 2020. Geology of the Souter Head subvolcanic complex, Aberdeenshire, Scotland: An Ordovician granite-related Mo-(Bi-As-Au) system. *Earth and Environmental Science Transactions of the Royal Society of Edinburgh* 1–18. doi:10.1017/S1755691019000161.
- Seedorf, E., Dilles, J. H., Proffett Jr, J. M., Einaudi, M. T., Zurcher, L., Stavast, W. J. A., Johnson, D. A. & Barton, M. D. 2005. Porphyry deposits: characteristics and origin of hypogene features. *Economic Geology*, 100<sup>th</sup> Anniversary Volume, 251–98. <https://pubs.geoscienceworld.org/books/book/1940/chapter/107713475/Porphyry-Deposits-Characteristics-and-Origin-of>
- Selby, D., Creaser, R. A. & Feely, M. 2004. Accurate and precise Re-Os molybdenite dates from the Galway Granite, Ireland. Critical comment on 'Disturbance of the Re-Os chronometer of molybdenites from the late-Caledonian Galway Granite, Ireland, by hydrothermal fluid circulation' by Suzuki et al. *Geochemical Journal* **35**, 29–35.
- Selby, D. & Creaser, R. A. 2001. Re-Os geochronology and systematics in molybdenite from the endako porphyry molybdenum deposit, British Columbia. *Economic Geology* **96**, 197–204.
- Selby, D. & Creaser, R. A. 2004. Macroscale NTIMS and microscale LA-MC-ICPMS Re-Os isotope analysis of molybdenite: testing spatial restrictions for reliable Re-Os age determinations and implications for the decoupling of Re-Os within molybdenite. *Geochimica et Cosmochimica Acta* **68**, 3897–908.
- Soper, N. J., Ryan, P. D. & Dewey, J. F. 1999. Age of Grampian orogeny in Scotland and Ireland. *Journal of the Geological Society, London* **156**, 1231–36.
- Spray, J. G. & Dunning, G. R. 1991. A U/Pb age for the Shetland Islands oceanic fragment, Scottish Caledonides: evidence from anatectic plagiogranites in 'layer 3' shear zones. *Geological Magazine* **128**, 667–71.
- Stewart, E. M., Baxter, E. F. & Ague, J. J. 2017. Initiation and duration of Grampian orogenesis constrained by refined Sm-Nd garnet geochronology of the Ballantrae ophiolite, Scotland. *Journal of the Geological Society* **174**, 968–78.
- Strachan, R. A., Smith, M., Harris, A. L. & Fettes, D. J. 2002. The Northern Highland and Grampian terranes. In Trewin, N. H. (ed) *The geology of Scotland*, 81–147. <https://pubs.geoscienceworld.org/books/book/1524/The-Geology-of-Scotland>
- Suzuki, K. 2004. Reply to 'Accurate and precise Re-Os molybdenite dates from the Galway Granite, Ireland' by D. Selby et al.: critical comment on 'Disturbance of the Re-Os chronometer of molybdenites from the late-Caledonian Galway Granite, Ireland, by hydrothermal fluid circulation'. *Geochemical Journal* **38**, 295–98.
- Suzuki, K., Feely, M. & O'reilly, C. 2000. Disturbance of molybdenites from the late-Caledonian Galway Granite, Ireland, by hydrothermal circulation. *Geochemical Journal* **35**, 29–35.
- Tanner, P. W. G. 2014. A kinematic model for the Grampian Orogeny, Scotland. In Corfu, F., Gasser, D. & Chew, D. (eds) *New perspectives on the Caledonides of Scandinavia and related areas*, 390, 467–511. Geological Society of London Special Publication. <https://sp.lyellcollection.org/content/390/1/467/tab-figures-data>
- Viete, D. R., Oliver, G. J. H., Fraser, G. L., Forster, M. A. & Lister, G. S. 2013. Timing and heat sources for the Barrovian metamorphism, Scotland. *Lithos* **177**, 148–63.
- Viete, D. R., Richards, S. W., Lister, G. S., Oliver, G. J. H. & Banks, G. J. 2017. Lithospheric-scale extension during Grampian orogenesis in Scotland. In Law, R. D., Butler, R. W. H., Holdsworth, R. E., Krabbendam, M. & Strachan, R. A. (eds) *Continental tectonics and mountain building: the legacy of Peach and Horne*, 335, 121–60.

- Geological Society, London, Special Publications. <https://sp.lyellcollection.org/content/335/1/121>
- Volkenning, J., Walczyk, T. & Heumann, K. G. 1991. Osmium isotope ratio determinations by negative ion mass spectrometry. *International Journal of Mass Spectrometry Ion Processes* **105**, 147–59.
- Vorhies, S. H., Ague, J. J. & Schmitt, A. K. 2013. Zircon growth and recrystallisation during progressive metamorphism, Barrovian zones. *Scotland American Mineralogist* **98**, 219–30.
- Vorhies, S. H. & Ague, J. J. 2011. Pressure-temperature evolution and thermal regimes in the Barrovian zones, Scotland. *Journal Geological Society of London* **68**, 1147–66.
- Wendt, I. & Carl, C. 1991. The statistical distribution of the mean squared weighted deviation. *Chemical Geology: Isotope Geoscience Section* **86**, 275–85.
- Yang, X.-M. 2017. Estimation of crystallization pressure of granite intrusions. *Lithos*, 286–87, 324–29. <https://www.sciencedirect.com/science/article/abs/pii/S0024493717302293>

---

MS received 28 June 2019. Accepted for publication 24 April 2020. First published online 8 July 2020